CCF Transactions on Pervasive Computing and Interaction (2022) 4:437–451
https://doi.org/10.1007/s42486-022-00120-7

REGULAR PAPER

RetroFlex: enabling intuitive human–robot collaboration with flexible retroreflective tags

Wei Li[1] · Tuochao Chen[2] · Zhe Ou[1] · Xin Wen[3] · Zichen Xu[3] · Chenren Xu[1]

Received: 31 August 2022 / Accepted: 26 September 2022 / Published online: 28 November 2022

Abstract

Efficient and seamless human–robot collaboration relies on carefully-designed user interfaces to relieve the users from heavy mental stress and burden. Current marker-based intuitive interfaces suffer from reduced reliability in a noisy environment, non-scalable wireless connections, and fixed form factors with limited data capacity, which limit the efficiency of real-world applications where frequent and seamless target switching is required. We propose RetroFlex, a flexible retroreflective communication system that enables fluent and intuitive human–robot collaboration. RetroFlex integrates robots with a flexible tag (FlexTag) and leverages visible light backscatter communication to exploit the intrinsic user spatial context to retain the intuitiveness in the interaction process. The users can interact with multiple target robots in a point-and-control manner, which significantly lowers the workload and improves the overall experience. Our evaluation reveals that RetroFlex is able to support room-scale tasks with commodity smartphones with a bit rate of 60 bps at a distance up to 2.5 m and a view angle up to 70° while being robust to different environmental noises. A usability study with 12 users and two real-life tasks demonstrates that our system offers a fluent and satisfying multi-target control experience.

Keywords Intuitive interfaces · Human–robot collaboration · Flexible tags · Visible light backscatter communication

1 Introduction

Human–robot collaboration is widely adopted in industrial production (Villani et al. 2017), scientific research (Islam et al. 2019) and filming (Brantner and Khatib 2021), which combines the advantages of robots (i.e., high accuracy, speed, and repeatability) and the flexibility of human workers (i.e., being able to handle unforeseen events and dynamically adjusting the operations). The key enabler of a natural human–robot interaction is an intuitive user interface that blurs the boundary between the user and the target machine, helping the user to concentrate on his tasks and goals instead of frequently getting distracted to handle the extra workload caused by target switching and command inputting. In recent years the rapid progression in these technologies has brought a plethora of more efficient and intuitive interaction schemes such as gestures (Yang et al. 2007; Van den Bergh et al. 2011; Qin et al. 2021), speech (Grasse et al. 2021; Bonarini 2020), and augmented/virtual reality (Walker et al. 2018; Hedayati et al. 2018; Quintero et al. 2018) that break through the bottleneck of traditional methods such as handheld terminals and mechanical controllers.

✉ Chenren Xu
chenren@pku.edu.cn

Wei Li
motren909@163.com

Tuochao Chen
ctc1998@uw.edu

Zhe Ou
andy-ozer@stu.pku.edu.cn

Xin Wen
XinWen@email.ncu.edu.cn

Zichen Xu
xuz@ncu.edu.cn

[1] School of Computer Science, Peking University, No. 5 Yiheyuan Road, Haidian District 100871, Beijing, China

[2] Paul G. Allen School of Computer Science and Engineering, University of Washington, 1410 NE Campus Parkway, Seattle, WA 98195, USA

[3] School of Mathematics and Computer Science, Nanchang University, No. 999 Xuefu Road, Nanchang 330031, Jiangxi, China

As of today, this collaboration scheme has been polished well enough to a simple two-step manner: communication after identification. The target is first identified by an onboard barcode marker, then the control commands are selectively transmitted in Wi-Fi, Bluetooth, or other radio-frequency (RF) wireless channels to the target robots as per the target identity. Although this capability of quickly identifying the target and sharing data ensures the two-step method has a fluent interaction experience, it does not scale to collaboration tasks with multiple robots. The reasons are two-fold: First, current barcode markers only offer a static identity in the form of a short text string, necessitating pre-established network connections to deliver control commands with more dynamic data. However, this kind of connection has limited efficiency in more ad-hoc and opportunistic collaborations scenarios where the user needs to frequently switch between multiple targets. Second, as current QR code-like markers are originally used as planar fiducials for localization purposes instead of communication, they tend to have large and rigid form factors, which limits their ability to adapt to irregular and often curved robot surfaces to serve collaboration scenarios. The main drawback of these RF methods is that they fail to explore the intrinsic *spatial context* of the user (i.e., location and orientation) to shrink the scope of interest and speed up target selection, and thus inevitably fall into a two-step manner that significantly limits the overall interaction efficiency.

We propose RetroFlex, the first flexible retroreflective communication system targeted at intuitive and efficient human–robot collaboration. RetroFlex tackles the aforementioned challenges with two novel designs: (1) a flexible retroreflective tag for visible light backscatter communication (VLBC) that can directionally deliver highly dynamic data with the Polymer Dispersed Liquid Crystal (PDLC) technology. The thin and flexible PDLC film is able to deliver data without a pre-established connection but totally in the optical channel by changing between opaque and transparent states according to the applied voltage, while being able to stick to non-planar surfaces due to a flexible form factor; (2) a multi-pixel vision-based software pipeline that exploits the optical characteristics of PDLC to achieve robust tracking and connection-free communication. The slow response time of the PDLC (several milliseconds), the unpredictable deformation of the tag, and the commonly noisy optical environment pose challenges to successfully decoding the information. We design a pixelated spatial encoding scheme and a vision-based deformation-resilient software pipeline for robust decoding, which also merges identification and communication steps into one step to achieve a quick target switching ability for minimizing the user's workload.

In essence, RetroFlex uses a LED-enabled reader device to realize bi-directional communication with robots integrated with a flexible tag. The goal of RetroFlex is to boost the efficiency of multi-target human–robot collaboration scenarios. For example, for underwater research or filming missions that require real-time robot parameter updating for vehicle maneuvering (Enan et al. 2022) or teleoperations (Almeida et al. 2017), traditional methods require the divers to use hand gestures combined with visual barcode tags (Islam et al. 2018) to alter the robot parameters. However, in a multi-target collaboration scenario, the onboard cameras of other robots will also capture the gestures and thus get confused about the real target. With RetroFlex, however, the divers are able to directly employ the VLBC data link to communicate with the FlexTags integrated onto the surface of target robots. This optical link has the merit of line-of-sight (LOS) transmitting, which means the signal only travels in a manner consistent with the user's attention area and thus removes the target ambiguity. Besides, switching between multiple targets is no longer cumbersome. The diver only needs to point his reader (e.g., searchlights or hand-held controllers) to the target and complete the subsequent actions, and casually point to another one when needed. This point-and-control scheme brings a more fluent, intuitive, and efficient interaction experience. The advantages of RetroFlex compared with other methods are summarized in Table 1.

We built a prototype system using off-the-shelf and low-cost components. We conducted a comprehensive evaluation study of the system performance under different conditions (i.e., view distance, view angle, flashlight frequency, lighting condition). The results show that our tag offers reliable bidirectional connectivity with a bit rate of 60 bps at a communication distance up to 2.5 m and a view angle of 70° under different indoor ambient lighting conditions, which is sufficient for common room-scale collaboration tasks. We also conducted a usability study mimicking real-world human–robot collaboration scenarios with 12 participants to demonstrate the application scenarios and evaluate the usability of our system, which shows that our system offers a fluent collaboration experience.

Table 1 The advantages of RetroFlex in human–robot collaboration tasks compared with other methods

Method	Bluetooth/ WiFi	RFID	Visual marker	RetroFlex
Range	10 m, 360°	10 m, 360°	3 m, 80°	**2.5 m, 70°**
LOS	✗	✗	✓	✓
Form factor	Rigid	Rigid	Rigid	**Flexible**
Scalability	Low	Low	Mid	**High**
Efficiency	Low	Low	Mid	**High**

Bold column is for stressing the advantages of the proposed RetroFlex system. Non-bold parts belong to traditional methods

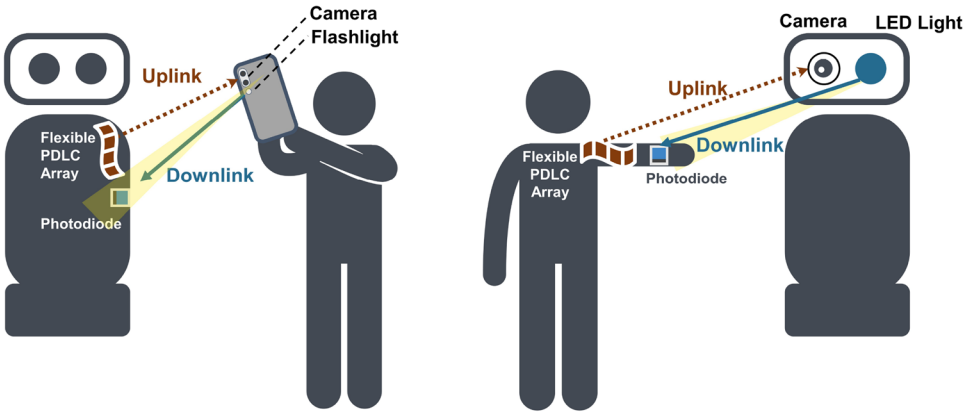

Fig. 1 Two example scenarios of RetroFlex. Left: Users use mobile readers to share data with robots in a point-and-control manner. Right: The users equip the flexible FlexTag on their clothes and perform gesture-based teleoperation

To summarize, the contributions of our paper are as follows:

- We present RetroFlex, the first PDLC-based flexible retroreflective communication system that can be integrated with irregular robot surfaces to readily offer an instant target selection and interaction ability for improving the fluency and efficiency of human–robot collaboration tasks.
- We propose a robust and efficient software pipeline that exploits the optical characteristics of PDLC to achieve robust tracking and communication against challenging environments such as ambient light noise, glare, and tag deformation.
- We evaluate the proposed method with a comprehensive system evaluation and a usability study mimicking real-world human–robot collaboration scenarios, which shows that RetroFlex is able to serve room-scale tasks for collaboration with a seamless interaction experience.

2 System design

As shown in Fig. 1, our design goal is to enable robust bidirectional optical communication between a reader (ViReader), and our flexible PDLC-based tag (FlexTag). The optical channel formed by these two components leverages the line-of-sight (LOS) property of light beams to instantly shrink the scope of candidate targets into those in the field-of-view (FoV), while a pure connection-free data link is also established to bidirectionally deliver dynamic data without the overhead of establishing connections. In this way, both the target selection and the interaction process that features frequent target-switching can be accelerated. The basic workflow of bidirectional communication is as follows:

1. Downlink: The ViReader first transmits a message by blinking the onboard LEDs. After that, the photosensor on the FlexTag captures and decodes the received optical signal.
2. Uplink: The ViReader keeps the light on to provide carrier beams, which are then backscattered by the retroreflector. Meanwhile, the FlexTag encodes the returned data into backscattered light by manipulating the transmittance of the PDLC films to create bright and dark patterns. The modulated backscattered light is then captured by the camera at the ViReader, and fed into the software pipeline for information extraction.

The whole system can be separated into two self-contained functional blocks, namely the hardware suite and the software pipeline. These two components work in concert with each other to realize intuitive human–robot interaction. In the rest parts of this section, we will elaborate on the two components respectively.

2.1 FlexTag hardware design

FlexTag, as shown in Fig. 2, is a fully-functional transceiver specially designed with both a transmitting unit and a receiving unit, upon which a modulation scheme is applied to realize bidirectional retroreflective communication. We now describe each of these building blocks.

2.1.1 Receiving unit

The main function of receiving hardware is to extract and process the downlink information from the incident light. During downlink, the ViReader encodes the packet using Manchester code and sends it by blinking the LED on it. At the beginning of the downlink packet, we add some preamble to help the tag to identify the downlink packet. In FlexTag, we deploy the photo-diode (BPW34) as the photosensor to convert the incident light signal to the photocurrent. Then a trans-impedance amplifier is deployed to convert the photocurrent into a photovoltage, followed by

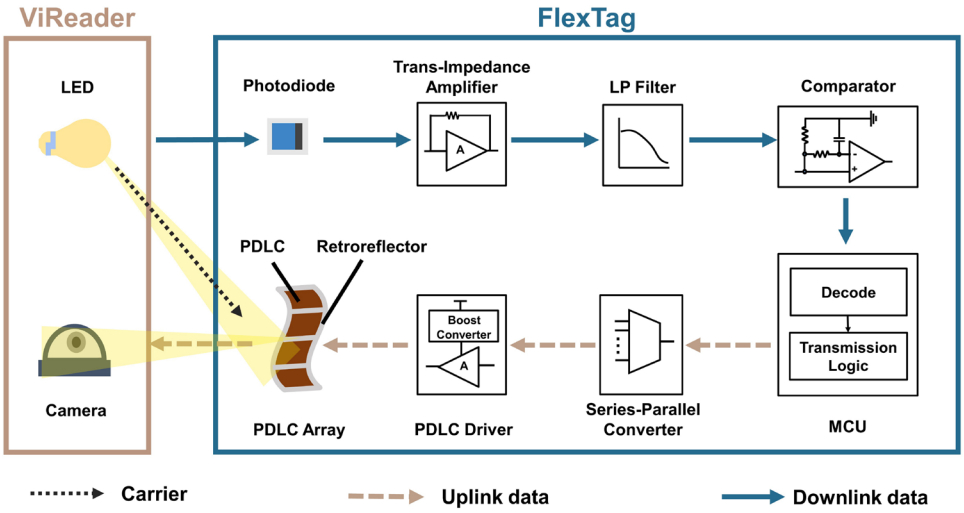

Fig. 2 Diagram of FlexTag

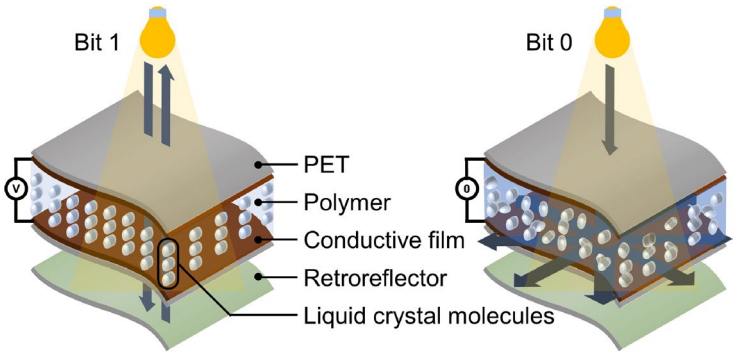

(a) The anatomy of a PDLC modulator. Left: When voltage is applied, The liquid crystal molecules remain in order and allow the light beams to pass through, which are then reflected by the retroreflector layer. Right: When no voltage is applied, The liquid crystal molecules become out of order and block the light beams.

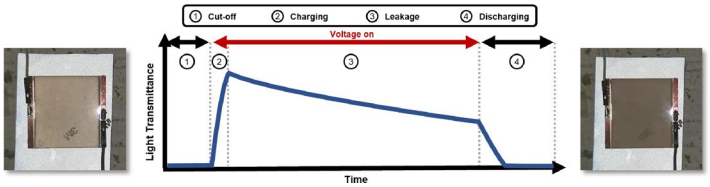

(b) The four stages of light transmittance change of a charged PDLC film.

Fig. 3 Working mechanism and characteristics of the PDLC modulator

a 2-order Sallen-Key low-pass filter with a 200 Hz cut-off frequency to filter out high-frequency noise. Finally, a comparator (TLV7031) converts the analog signal into a digital signal and feeds it into the MCU for decoding.

2.1.2 Transmitting unit

In the PDLC array, we deploy several PDLC films on one layer of retro-reflector to improve link throughput proportionally. We denote each PDLC film with the retro-reflector below as one PDLC pixel. Then we introduce the driving circuits to generate the driving voltage for each PDLC film in the array. Firstly, MCU (STM32F401) generates an uplink packet and outputs the data using the SPI interface. Then we use the serial conversion parallel chip (SN74LV595APWR) to convert the SPI serial signal into 4 parallel signals for 4 PDLC films. Since the typical drive voltage for one PDLC film is greater than 10 V, we design a DC-DC boost circuit (TPS61085PWR) to produce an 18 V voltage source. Finally, 4 high-voltage comparators (TLV1805DBVR) convert our signal from a serial-parallel conversion circuit from 3 V into 18 V to drive the PDLC film.

Table 2 Four transmittance changing stages from the results of the pre-experiment

Stage	Description
Cut-off stage	At first, when no voltage is applied, the PDLC film is in the original state, the internal liquid crystal molecules are in a disordered state, and the transmittance is minimal
Charging stage	When voltage is applied, due to the effect of the electric field, the liquid crystal molecules begin to align up along the direction of the electric field, and the transmittance rises rapidly until reaching the peak
Leakage stage	After the transmittance reaches the maximum, even if the voltage still persists, the ever-weakening electric field gradually fails to tame the liquid crystal molecules and entails a reducing transmittance
Discharging stage	When the voltage is removed, the liquid crystal molecule accelerates back into disorder, and the speed of the light transmittance drop also begins to accelerate

2.1.3 PDLC modulation scheme

As shown in Fig. 3a, PDLC (polymer dispersed liquid crystal) is a flexible film-like material, whose light transmittance changes with the voltage applied. The center of PDLC film is a layer of polymer substrate whose interspace is filled with liquid crystal molecules. The polymer layer is sandwiched by 2 layers of conductive films, which are sheet-like polyester films coated with indium tin oxide (ITO) conductive layer for generating an electric field in the center layer and controlling the liquid crystal molecules. The outermost layer is the transparent polyethylene terephthalate (PET) layer for insulation. When voltage is applied to the PDLC film, more precisely the two conductive ITO layers, both the liquid crystal molecules and their optical axis will be neatly arranged along the direction of the electric field. In this way, the passing light beams are hardly scattered, which leads to a high light transmittance and manifests a transparent appearance. On the other hand, when no voltage is applied, the liquid crystal molecules lose order and are randomly scattered inside the polymer. The light beams are thus easily blocked and scattered along random directions without passing through the film, which brings a lower transmittance and turns the film opaque. We leveraged these characteristics of the PDLC film to achieve a novel retroreflector-based modulation scheme. Combing the transmittance control of the PDLC film and the retroreflector, the brightness of a pixel can be manipulated. We put a layer of retro-reflector under the PDLC film. When the voltage is applied, most of the light can pass the PDLC film and retroreflected by the retro-reflector, which makes this PDLC pixel brighter. When the voltage is off, most of the incident light is scattered by the PDLC, which makes this PDLC pixel darker. We now obtain an analog representation of two logical values with the change of brightness.

To embed data bits into these pixels, the most straightforward way is to use high voltage to represent bit 1 and low voltage for bit 0. However, we find a unique characteristic of the PDLC material. Like other LC devices, PDLC material has a charging time and discharging time, indicating the time of LC molecules from disorder to order and the time of LC from order to disorder. In order to explore the optical properties (light transmittance) of flexible PDLC film during charge and discharge, a simple pre-experiment was carried out on a single PDLC pixel.

The results reflect the change of transmittance with respect to the applied voltage, which is shown in Fig. 3b and summarized into four stages in Table 2. When the voltage is applied to the PDLC, rather than in a linearly increasing trend, the change of PDLC light transmittance is non-linear and has a special leakage stage. In this stage, even if the voltage persists, the transmittance still decreases. This indicates that if we simply use high voltage to represent bit 1, the transmittance drop and the corresponding brightness drop will confuse with that of bit 0. To tackle the leakage effect, we employ digital pulse modulation. A pulse with a certain duty cycle is transmitted for bit 1 and remains low voltage for bit 0. So, on the demodulation side, we can judge the bit 0 and 1 by detecting the brightness peak of PDLC pixels. Also, to achieve clock synchronization, for each transmission a pre-designed preamble is sent to the decoder to determine the inter-symbol duration and thus windowing the overall signal into separate symbols.

We design the prototype FlexTag as per the rationales above. In consideration of the tag size and throughput demand, we build a 4×1 PDLC array with the entire size of 10 cm $\times$ 4 cm so that it can be easily integrated onto irregular surfaces. The implementation of the FlexTag is shown in Fig. 4.

2.2 Noise-resilient software pipeline

The FlexTag and its components work in concert with a software pipeline to achieve a bidirectional communication resilient to ambient noise and tag deformation. To achieve this, there are three design challenges for the pipeline: (a) how to robustly detect and decode the tag in a complex background with various ambient light sources. (b) how to counter and eliminate the deformation of the flexible tags and robustly restore the

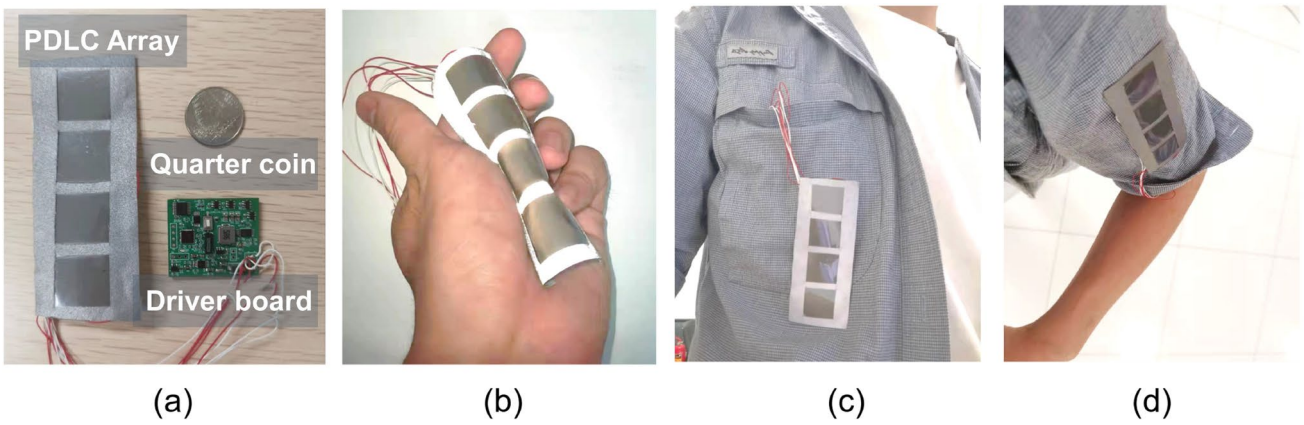

Fig. 4 The implementation of the FlexTag. **a** The flexible array has a small driver board about the size of a quarter coin. **b** The FlexTag can be easily bent to fit irregular surfaces. **c**, **d** The FlexTag can be integrated into normal clothes

Fig. 5 The detection and data extraction process

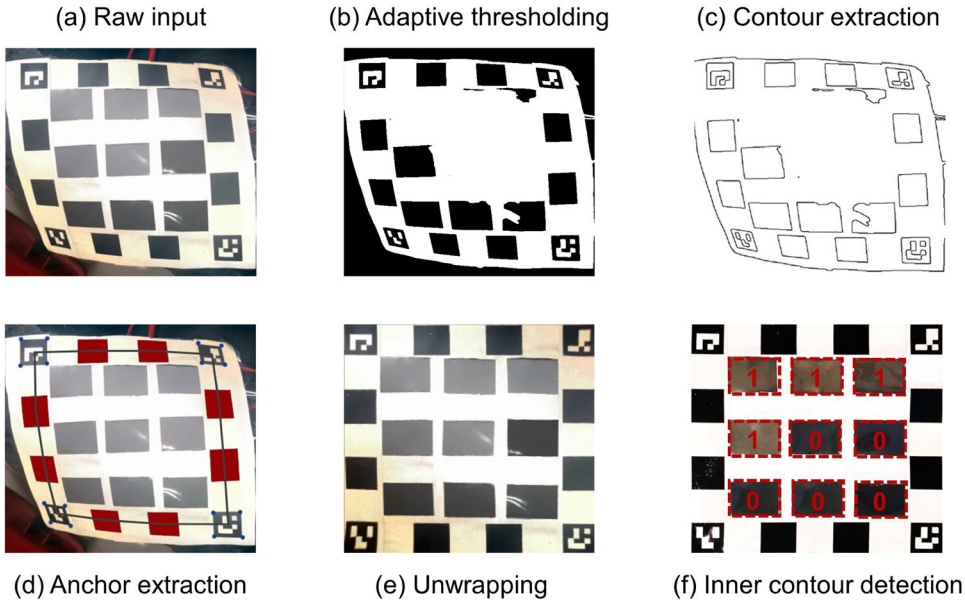

embedded data. (c) how to deal with the limited dynamic range of brightness of the PDLC pixels due to variations in spatial pose and ambient light conditions. We tackle these challenges with a two-phase algorithm including a detection phase and a decoding phase, which is described in detail below.

2.2.1 Detection phase

As shown in Fig. 5b, We begin with an adaptive thresholding algorithm to binarize the raw image and segment the tag, as the adaptive thresholding can accommodate changing lighting conditions in the image. Then all the contours are extracted from the thresholded image as shown in Fig. 5c. After that, we apply the Douglas-Peucker approximation algorithm (Douglas and Peucker 1973) to fit the extracted complex contours to the simple contours with fewer points. In this way, the effect of contour bending can be reduced. At last, we filter out contours that are not in an ideal rectangular shape or have an inappropriate size as shown in Fig. 5d. We finally acquire all the anchoring points on the deformed tag.

After the tag candidate detection, it is necessary to determine if they are the real FlexTag by analyzing their inner pattern. This step starts by extracting the inner pattern of each marker. To do so, a perspective transformation is first applied to unwrap the deformed image in Fig. 5e. Then, we extract the inner contours of this candidate and apply a similar filtering strategy that rules out mid-sized or misshaped pixels by the following criteria: (1) the number of valid inner contours equals the number of PDLC pixels in the tag; (2) the sizes of the inner contours are appropriate;

(3) the relative positions of the inner contours are consistent with the PDLC array in the tag.

2.2.2 Decoding phase

After detecting, we acquire the spatial position of each PDLC pixel and record the average brightness change over time. As we mentioned before, since each PDLC pixel has a different spatial location and different ambient light conditions, the brightness variation range of each PDLC pixel is different, which will greatly affect the accuracy of our decoding. So, we need to normalize the brightness of each PDLC pixel. Our method is to add a preamble with a few bits to the beginning of the data packet for each PDLC pixel. Since the preamble sequence is already known, we use the preamble waveform template to match the received brightness change signal by calculating their correlation during uplink transmission. In this way, we can find the preamble bits in the brightness curve and determine the beginning of the uplink data packet. Through the preamble, we can also determine the inter-symbol interval and enhance complete clock synchronization. After that, we measure the maximum brightness and minimum brightness of these preambles and use them to normalize the brightness curve of the coming data packets. Finally, we use the peak searching algorithm to find out valid peaks in the brightness curve. A time slot is considered as a bit 1 if there is a peak detected.

3 System evaluation

We conducted a system evaluation to evaluate the performance of RetroFlex under various scenarios.

3.1 Evaluation setup

We use Huawei P30 Pro as our ViReader throughout the experiments. The frame rate and resolution of the camera are 60 fps and 720p. The FlexTag was placed vertically in front of a complex background, and the smartphone was mounted on a tripod facing the tag. We evaluated the downlink and uplink performance under different conditions regarding the distance, angle, light condition, and data rate. There are three light conditions in the experiments, which are (1) next to a window with direct sunlight (referred to as day light, 1000 lux), (2) in a typical office with artificial lighting (referred to as office light, 400 lux), and (3) in a room with minor natural light (referred to the as dark chamber, 100 lux). We used the flashlight to send a randomly generated downlink packet (8-bit preamble and 128-bit payload) to the tag and drove the PDLC array to send a randomly generated uplink packet (8-bit preamble and 128-bit payload) to the camera. Each downlink and uplink transmission is repeated for 10 rounds. For the evaluation metric, we adopted the mean Bit Error Rate (BER) for both downlink and uplink. The BER can be calculated as follows:

$$Mean(BER) = \frac{1}{m}\sum_{i=1}^{m}\frac{N_s(i)}{N_t(i)} \quad (1)$$

where, m = Total number of rounds; $N_s(i)$ = Number of bits successfully received and decoded in the ith round; $N_t(i)$= Number of bits transmitted in the ith round.

3.2 Uplink evaluation

3.2.1 Data rate

The first experiment is the effect of data rate at different distances. In this experiment, our experimental light condition is under office lighting, and the communication angle is kept at 0°. Then we change the driving pulse frequencies of the PDLC to 7.5 Hz, 10 Hz, and 15 Hz respectively. Because our PDLC array has 4 pixels, the corresponding uplink data rates are 30 bps, 40 bps, and 60 bps. Then we send the uplink packet at 5 different distances for each data rate and calculate their average BER as shown in Fig. 6a. When can see that if a criterion of 10^{-1} is selected, RetroFlex can communicate at a distance up to 2.5 m. A lower data rate brings a minor improvement to the overall bit error rate.

3.2.2 Communication angle

The second experiment mainly explores the effect of the communication angle between the PDLC reader and the PDLC tag on the uplink performance. In this experiment, the light condition is under office lighting, and the communication distance is kept at 1 m with a 40 bps data rate. We can see that when the angle is less than 35°, the bit error rate is lower than 1%. As shown in Fig. 6b, when the communication angle exceeds 35°, the bit error rate increases, resulting in lower downlink reliability. Therefore, the angle range in which our uplink link can work stably is around 35°.

3.2.3 Light condition

In the third experiment, we mainly measure the influence of ambient light conditions on our uplink performance. In the experiment, we maintain the uplink data rate of 40 bps and the communication angle at 0°. We tested the uplink at 6 different distances. As shown in Fig. 6c, we measured that our stable communication distance is about 2.3 m near the sunny window, 2.2 m under the artificial light source (fluorescent lamp), and 2.5 m under the darkroom. The result shows that

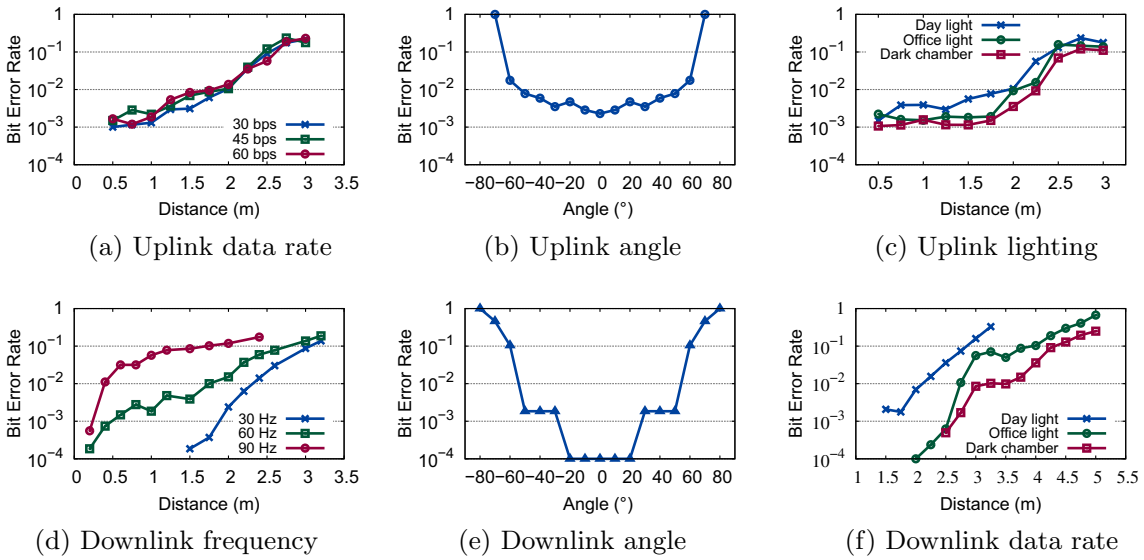

(a) Uplink data rate (b) Uplink angle (c) Uplink lighting

(d) Downlink frequency (e) Downlink angle (f) Downlink data rate

Fig. 6 System evaluation results

the working distance of the system is sufficient for normal room-scale collaboration tasks.

3.3 Downlink evaluation

3.3.1 Blink frequency

The first experiment explores the influence of downlink data rate (blink frequency of flashlight in smartphone) and communication distance on downlink performance. In this experiment, our experimental light condition is under office light, and the communication angle is kept at 0°. Then we change the flashing frequency to 30 Hz 60 Hz, and 90 Hz. For each data rate, we tested 10 different communication distances. As shown in Fig. 6d, we can see that the bit error rate increases gradually with the increase of distance. At the same distance, the higher the transmission rate leads to the higher the bit error rate. Specifically, the stable working distance is about 3.0 m for 30 Hz downlink, 2.5 m for 60 Hz downlink, and 2.0 m for the 90 Hz downlink.

3.3.2 Communication angle

The second experiment mainly explores the impact of the incident angle on the bit error rate. In this experiment, the light condition is under office light, and the communication distance is kept at 1 m with a 60 Hz flashlight frequency. As we can see, when the angle is less than 50°, the bit error rate is lower than 1%. As shown in Fig. 6e, when the communication angle is more than 50°, the bit error rate increases, resulting in low downlink reliability. Therefore, the angle range in which our downlink can work stably is less than 50°.

3.3.3 Light condition

The third experiment mainly explores the influence of different ambient light conditions on downlink communication performance. Then we keep our incident angle at 0° and the flashlight frequency is 60 Hz. Under each light condition, we tested the downlink at 10 different distances. The experimental results in Fig. 6f show that the stronger the ambient light intensity, the greater the noise interference and the greater the bit error rate. The stable communication distance is about 2.0 m in a room with sunlight, about 3 m in a room with an indoor artificial light source, and about 4 m in a dark room.

4 Usability study

While the system evaluation focuses on exploring communication performance, we also conducted a user study to evaluate its usability in real-life scenarios.

4.1 Study design

We designed two tasks for the study, each targeting an operating mode as in Fig. 1. Task 1 focuses on RetroFlex 's usability for multi-target interaction. Task 2 evaluated the performance and user feedback for a typical robot teleoperation system.

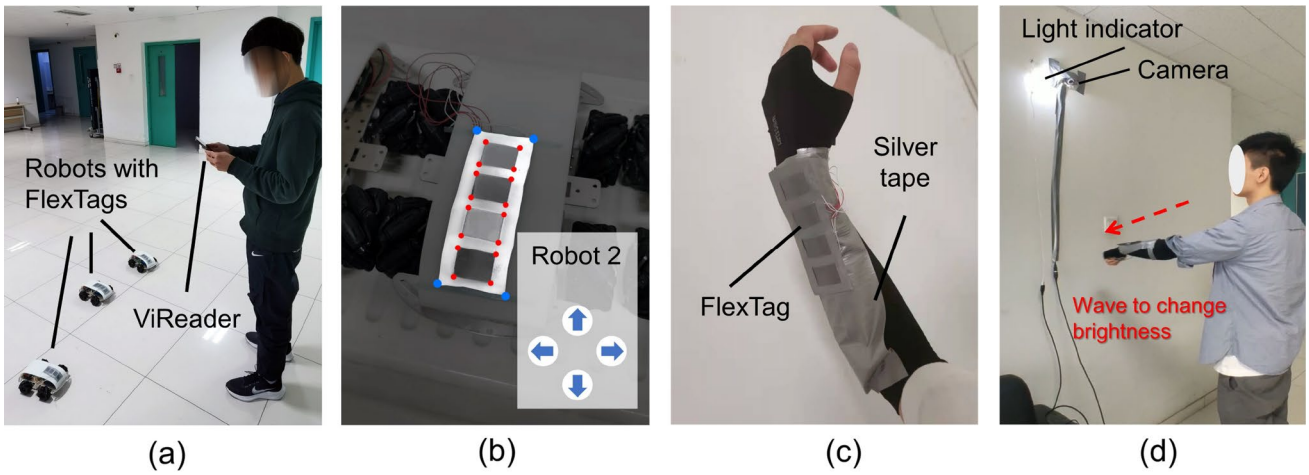

Fig. 7 Two usability study tasks. **a**, **b** Directional interaction with multiple robots. **c**, **d** Gesture-based teleoperation with integrated FlexTags

4.1.1 Task 1: directional interaction

The task emulates an interaction scenario where the user wants to send commands to the FlexTag on the robot while retrieving feedback to proceed. The goal is to evaluate the user experience when using RetroFlex in a multi-robot interaction scenario that requires frequent target switching. As shown in Fig. 7a, it includes two steps: downlink (send a request to the tag) and uplink (read identity from the tag). In the first step, the user needs to point the phone to one of the target robots and click the request button to send the request with the user name. In the second step, the tag sends the robot identity and the newly received user name back to the smartphone. Once this procedure is done, the user is authenticated by the robot and the Android app will display a virtual control menu overlayed to the tag as shown in Fig. 7b. The user needs to acquire all three robots' control menus and send one control command to each of them as fast as possible. We record and calculate the total interaction time as well as the communication bit error rate as the metrics.

4.1.2 Task 2: gesture-based teleoperation

In addition to the typical communication function as evaluated in task 1, we also explore the feasibility of using RetroFlex for gesture-based teleoperation. Users sit under the bulb and camera (around 2 m above users' arm) emulating a robot and put the sleeve integrated with FlexTag (see Fig. 7c) under the light for authentication. If the ID of FlexTag in the sleeve is valid (i.e., the user is an authenticated user), the smart bulb would flash for half a second. Then users can wave their hand to control the robot (Fig. 7d), which takes the form of changing the brightness of this light per the waving direction. We use the total success rate of identification and the interaction time as the metrics.

4.2 Setup and procedure

The setup of task 1 is the same as in the system evaluation. In task 2, we integrated an infrared camera with a drop light bulb as a simple prototype of RetroFlex-enabled robots, which are controlled by commands sent from a laptop. We recruited 12 participants (4 females, 8 males) from the local community, aged between 20 and 28. Participants are not experienced in intuitive robot interfaces and human–robot collaboration. Participants first got themselves familiarized with the system. Then, they started the study with Task 1, followed by Task 2. At the end of the study, participants completed a NASA-TLX and went through a brief interview about their user experience and subjective feedback. Each participant was compensated with a $15 gift card for their time. Upon finishing both 2 tasks, users complete a questionnaire with a Task Load Index (NASA-TLX) on a 7-point Likert scale.

4.3 Result

4.3.1 Communication performance

Table 3 summarizes the results of the two tasks. In task 1, the bit error rate for the downlink was 0.0 (0/2660 bits) and the bit error rate for the uplink was 0.3% (8/2400 bits). In addition, the identification failure times for the correct ID was only 2/60 and all the wrong IDs were successfully rejected by our RetroFlex. These results demonstrated the good performance and high robustness of RetroFlex for both visible light spectrum and infrared spectrum even in the user study.

We also measured the data exchange time of uplink, downlink, and identification. For the downlink (240 bits including the preamble), RetroFlex took 4.87 ± 0.22 s.

Table 3 User study results

Task index	Task type	Bit error rate (%)	Time (s)
1	Downlink	0.0	4.87 ± 0.22
	Uplink	0.3	6.07 ± 0.50
Task index	Task type	Identification success rate (%)	Time (s)
2	Correct ID	96.7	5.88 ± 0.38
	Wrong ID	100.0	5.88 ± 0.38

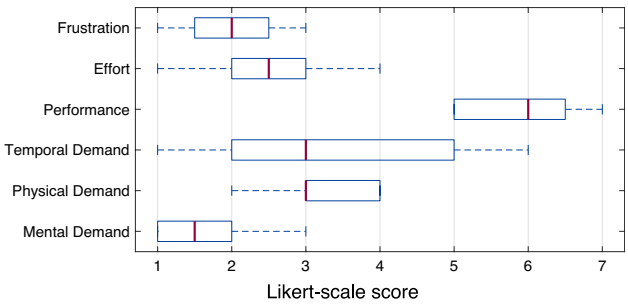

Fig. 8 Result of the questionnaire

As for the uplink (220 bits including the preamble), it took 6.07 ± 0.50 s. As for the identification (ID length is 168 bits including the preamble), RetroFlex took 5.88 ± 0.38 s. Our analysis revealed that the bottleneck of the time was the low bit rate. Take the uplink as an example, the data transmission took 220 bits/40 bps = 5.50 s, while the CV-based demodulation and AR interface render latency took only 0.57 s. Therefore, to further lower the time consumption and improve the user experience, we need to improve the data rate for both uplink and downlink. We discuss some potential methods in Sect. 5.3.

4.3.2 NASA-TLX result

Overall, users reported that RetroFlex required a small mental (median = 1.58) and physical load (median = 2.99) when completing the tasks (see Fig. 8). Moreover, users agreed that they had good performance (median = 6.00), with little effort (median = 2.49) or frustration (median = 2.0). Our result suggests that RetroFlex offers a fluent human–robot collaboration with low mental and physical load.

4.3.3 Subjective feedback

P9 mentioned that "removing the wireless connection for interaction is a great idea as it is difficult to manage the network of many robots, while a VLBC method like RetroFlex is really fluid and seamless when switching between them." P4 and P7 stated that the flexible tag in RetroFlex was very interesting and visually attractive when integrated with the robot surfaces. Participants have mixed feelings about using the flashlight as the downlink source. P6 mentioned that "leveraging the flashlight minimizes the users' effort to use the system, as no additional hardware is needed." P2 and P11 mentioned that the flashlight might be obtrusive to the user, and an infrared solution may solve the problem. Overall, participants gave positive feedback on the FlexTag, especially on the point-and-control interaction scheme enabled by the directional data link between the user and the tag.

5 Discussion

5.1 Power consumption

Currently, we measure the power consumption of the tag using a Digital Multi-meter called DMM6500. The entire power consumption of the tag is around 18 mW. the tag can run on a standard 1740 mAh lithium-ion battery for over three months. We find the majority part of the energy is consumed in the PDLC driving circuits. By measurement, the power consumption of each PDLC pixel is around 3 mW (4 pixels have already consumed 12 mW). Even if this power consumption is much lower than a single common SMD LED or the OLED of the same size, we still need to lower this power consumption to sub-mW or µW for longer battery life and even battery-free. We look up the datasheet of the driving comparators (TLV1805DBVR) and find that its typical quiescent current is around 135 µA. However, our drive voltage for PDLC is high (18 V), which means only the quiescent power arrives at 2.43 mW. So, one way to lower power consumption is to lower the quiescent power of the PDLC driving circuits. Since it is hard to find another high-voltage (18 V) comparator with a lower quiescent current in the market, one potential solution is to directly use BJT or MOSFET to drive the PDLC instead of high-voltage comparators to reduce inessential quiescent current.

In addition to optimization of the hardware design, we can also lower the average power consumption by introducing the power management strategy. For example, when the

tag does not receive any downlink request, the driving circuits can be shut down and the tag enters sleeping mode with extremely low power consumption. Only when the tag receives the wake-up signal in the downlink will the tag turn on the driving circuits to send uplink data. For the MCU model used in the current prototype (STM32F401), the power consumption can be reduced to as low as 20 μW when all the unnecessary peripherals are shut down, which can enable the system to work for over 5 years on a standard 500 mAh Lithium-ion battery. For a working scheme with a relatively balanced tradeoff between wake-up and sleep mode, the average power consumption stays at a level of 2 mW, which translates to a working time of over 3 months on a standard Lithium-ion battery. Moreover, we can also add a solar panel and charging circuits to the tag to realize a carrier-powered design so that the tag can harvest energy from ambient light and further extend its battery life. One caveat is that because the energy conversion rate of solar panels is about 20%, and the maximum output power of a standard solar panel (G24I INDY4050) is hundreds of μW, a specially designed energy storage network is needed to properly manage the harvested energy. Also, to reach a usable output voltage level, the light intensity on the panel surface should reach almost 1000 lux, which requires the reader beams to have a narrow FoV and are perfectly aligned with the FlexTag. The constant carrier lighting also increases the reader's power consumption. These introduce more challenges including mechanical and optical engineering, in-depth power management design, and skilled circuit layouts that are beyond the scope of this paper, and we leave this battery-free version in our future work.

5.2 RetroFlex versus other marker systems

Barcode has been one of the mainstream markers for localization and several sensing-based collaboration tasks such as underwater exploration, AR-based mechanical repairing, and medical training, due to its low cost and easy deployment. RetroFlex does not aim at replacing barcodes. Instead, RetroFlex provides a better choice in scenarios that need better dynamic data sharing, a more focused operation region of interest, and the capability to instantly switch between multiple targets. For example, RetroFlex enables a diver to simultaneously control multiple underwater unmanned autonomous vehicles (UAV) by looking at them and sending separate commands. Compared to scanning a barcode or selecting on a terminal, RetroFlex provides a more fluent and intuitive target switching capability and thus increases the overall efficiency. Besides, the design with PDLC and retroreflective coating provide a less obtrusive visual feature, which can be easily merged into the curved surfaces of these UAVs rather than altering the inner components. Moreover, bounding with RF-based wireless channels limits the potential of planar markers in target switching, and suffers from common RF issues such as spectrum scarcity and signal leakage. In scenarios such as opportunistic interaction with passing robots on an assembly line, establishing and maintaining robust wireless connections for each of them is non-trivial, which inevitably brings more overhead during the interaction, hence degraded efficiency and mental experience. With RetroFlex, however, the VLBC connection can be established locally between the tag and ViReader without connections to offer context-aware interaction, at the cost of slightly increased hardware expense and power consumption.

RFID is another technology that shows its strength in battery-free passive communication. Analogous to RetroFlex, an RFID reader provides continuous wave (CW) signals to the tags, which are then used for powering the integrated circuit. Part of the CW signals is then backscattered to the reader to realize a battery-free bi-directional communication. Although it has been deployed in scenarios such as unmanned cargo sorting (Baygin et al. 2022) and vending machines (Ramzan et al. 2017), its applications in robotics are still constrained to positioning and localization (Magnago et al. 2019; Bernardini et al. 2020). The potential for interaction is underexplored due to the omnidirectional FoV of a reader. To reach a comparable working range and an energy-harvesting function, the power consumption can be as high as several watts on the reader side, which indicates sacrificing mobility for a power management system. This inevitably adds a burden to collaboration tasks that require the user to carry the reader for a long time, where lightweight hardware gadgets are preferred. However, We do believe that combining the LOS characteristic of VLBC to achieve fast target selection and large bandwidth of RFID will provide a powerful tool for future collaboration tasks.

5.3 Boosting the data rate

Currently, the data rate of RetroFlex is 60 bps for uplink and 60 bps for downlink, which needs to be further improved. For the downlink, the bottleneck lies in the smartphone flashlight. The flashlight in a smartphone is not originally designed for visible light communication. The light is not strong or focused enough, and the switching speed is low. Integrating an external lighting unit with a converged light beam and a high switching frequency could help to boost the downlink data rate. For the uplink, there are several reasons limiting the data rate. According to the Nyquist sampling theorem, the data rate for each PDLC pixel should be lower than half of the camera frame rate. So, one essential effort we need to try in the future is to deploy the camera with a higher frame rate (like 120 fps, or 960 fps) in the future. The slow response time of PDLC material is another limitation of the data rate. To push the limit, one way is to increase drive voltage. For example, increasing the driving voltage to around 60 V leads to a single-pixel data rate of 33.33 bps (Hu et al. 2020).

6 Related work

6.1 Intuitive interfaces for human–robot collaboration

Intuitive user interfaces are the key enabler of high-efficient and seamless human–robot collaboration. The users are able to control the robot with high-level behaviors instead of being involved in the robot language (Villani et al. 2017), which simplifies the interaction with robots while minimizing the user's errors and preserving situation awareness (Hancock et al. 2011; Keyes et al. 2010). Researchers have explored ways to use fiducial markers to deliver commands to a robot (Solvang et al. 2008), or plan the trajectory (Zhang et al. 2006) by a vision system. This method later develops to more advanced visual patterns such as laser light (Bonilla et al. 2012), 3D structured light (Hu et al. 2007), and pure robot appearance (Du and Zhang 2014). In recent years, the advances in augmented reality (AR) and virtual reality (VR) revolutionize traditional interfaces. Specifically, AR is used as a new programming scheme called robot programming using AR (RPAR) to replace traditional offline programming (Chong et al. 2009). This trend develops by combing with mobile devices such as tablets and smartphones to leverage the spatial context of the user to achieve fast and easy commanding and interaction tools (Mateo et al. 2014; Stadler et al. 2016), which significantly lowers the burden for easy and efficient human–robot collaboration to lay users.

RetroFlex preserves the advantages of the mobile device-based interface, namely easy and fluent control while refining the traditional localization-orientated rigid markers to be applied to versatile robots with irregular surfaces. The connection-free VLBC data link of RetroFlex also enables fast switching between multiple targets with a low mental workload for collaboration tasks.

6.2 Flexible switchable light modulators

Flexible switchable light modulators are flexible materials able to change the pass-through light intensity (Nathan et al. 2012), which includes three major categories: electrochromic (EC) (Lampert 1998; Granqvist et al. 2003), suspended particle (SPD) (Lampert 1998; Vergaz et al. 2007), and polymer dispersed liquid crystal (PDLC) (Lampert 1998; Doane et al. 1988). EC devices change their light absorption rate (Lampert 1998) at the cost of response time (several minutes), which entails a low data rate and is not favorable to our system. SPDs (Vergaz et al. 2007) change the orientation of rod-shaped particles to change the light transmittance but has limited durability and stability. PDLCs change the intensity of the light by applying an electric field to rotate liquid crystal droplets, which incurs an ms-level response time fast enough for communication. Existing studies on PDLC focus on its display function (Doane et al. 1988; Ahmad et al. 2018) while merely focusing on its communication ability. NLC (Hu et al. 2020) takes the lead to build a PDLC-based communication system, where PDLC films are integrated into the smart windows and embedded data into the natural light passing through. (Lai et al. 2019) presents a 3D-printed corner cube retro-reflector that is tunable through PDLC. This 3D-printed corner cube can reflect the incident light and the PDLC film can modulate the reflected light. However, they focus on smart building applications, and neither of their PDLC-based systems is flexible.

To the best of our knowledge, RetroFlex is the first system to demonstrate the feasibility of applying flexible PDLC material with retro-reflective communication ability for human–robot collaboration scenarios with high efficiency.

6.3 Visible light backscatter communication

Visible Light Backscatter Communication (VLBC) has been recently proposed as an emerging solution for IoT connectivity that saves 100x energy over active VLC and provides an inherent advantage in security and interference management compared to RF-based technology (Gummadi et al. 2007; Yang 2013; Punnoose et al. 2001). RetroVLC (Li et al. 2015) took the initiative in this field by employing the on-off keying (OOK) modulation on a single pair of a retroreflector and an LCD shutter. This technique was further extended by using multiple small LCD shutters to generate multi-level signals for PAM modulation schemes against channel capacity limitation (Shao et al. 2016). PassiveVLC (Xu et al. 2017) pushed the limit of symbol length with coding co-design to improve a 4× rate over OOK. RetroI2V (Wang et al. 2020) integrates optical tags into road signs and other infrastructure to offer parallel data links for vehicle-infrastructure collaboration at a distance up to 101 m. RetroTurbo (Wu et al. 2020) boosts the data rate of VLBC to a new level of 32 kbps by coordinating the state of liquid crystal modulators in both time and polarization domains.

RetroFlex adapts and refines the traditional VLBC model to serve human–robot collaboration scenarios. Compared to traditional VLBC design, RetroFlex features a PDLC-based flexible tag that can be integrated with irregular surfaces of robots to readily offer an instant and high-efficient interaction experience, which can significantly boost tasks that require frequent target switching commonly seen in collaboration scenarios.

7 Conclusion

In this paper, we proposed RetroFlex, the first flexible retroreflective communication system for intuitive human–robot collaboration, which can be integrated with

irregular surfaces of robots to readily offer a fluent and seamless interaction experience. The optical data link of RetroFlex leverages the spatial context of the user to provide an instant target selection function. A system evaluation experiment showed that RetroFlex could support reliable communication at a distance up to 2.5 m with a data rate of 60 bps and a view angle up to 70°. We also evaluated the usability and real-world experience of the system with two user studies representing common collaboration tasks such as multi-target directional interaction and gesture-based control. We further discussed the current limitations and future improvements for our system. We envision RetroFlex would provide a powerful alternative interaction scheme for intuitive and efficient human–robot collaboration in the future.

Supplementary Information The online version contains supplementary material available at https://doi.org/10.1007/s42486-022-00120-7.

Funding This study was funded by the National Natural Science Foundation of China (Grant No. 62022005, 62272010, 62061146001, and 62172008), ICT Grant CARCHB202017, and the Jiangxi Provincial Key R&D Program (Grant No. 20212BBE53004).

Declarations

Conflict of interest The authors have no competing interests to declare that are relevant to the content of this article. On behalf of all authors, the corresponding author states that there is no conflict of interest.

References

Ahmad, F., Jae Jeon, Y., Jamil, M.: Graphene-based polymer dispersed liquid crystals display—an overview. Mol. Cryst. Liq. Cryst. **669**(1), 46–60 (2018)

Almeida, L., Menezes, P., Dias, J.: Improving robot teleoperation experience via immersive interfaces. In: 2017 4th Experiment@ International Conference (exp. At'17), pp. 87–92. IEEE (2017)

Baygin, M., Yaman, O., Baygin, N., Karakose, M.: A blockchain-based approach to smart cargo transportation using UHF RFID. Expert Syst. Appl. **188**, 116030 (2022)

Bernardini, F., Buffi, A., Fontanelli, D., Macii, D., Magnago, V., Marracci, M., Motroni, A., Nepa, P., Tellini, B.: Robot-based indoor positioning of UHF-RFID tags: the SAR method with multiple trajectories. IEEE Trans. Instrum. Meas. **70**, 1–15 (2020)

Bonarini, A.: Communication in human–robot interaction. Curr. Robot. Rep. **1**(4), 279–285 (2020)

Bonilla, I., Mendoza, M., Gonzalez-Galvan, E.J., Chavez-Olivares, C., Loredo-Flores, A., Reyes, F.: Path-tracking maneuvers with industrial robot manipulators using uncalibrated vision and impedance control. IEEE Trans. Syst. Man Cybern. Part C (Appl. Rev.) **42**(6), 1716–1729 (2012)

Brantner, G., Khatib, O.: Controlling ocean one: human–robot collaboration for deep-sea manipulation. J. Field Robot. **38**(1), 28–51 (2021)

Chong, J.W.S., Ong, S., Nee, A.Y., Youcef-Youmi, K.: Robot programming using augmented reality: an interactive method for planning collision-free paths. Robot. Comput. Integrated Manuf. **25**(3), 689–701 (2009)

Doane, J., Golemme, A., West, J.L., Whitehead, J., Jr., Wu, B.-G.: Polymer dispersed liquid crystals for display application. Mol. Cryst. Liq. Cryst. **165**(1), 511–532 (1988)

Douglas, D.H., Peucker, T.K.: Algorithms for the reduction of the number of points required to represent a digitized line or its caricature. Cartogr. Int. J. Geogr. Inf. Geovisualization **10**(2), 112–122 (1973)

Du, G., Zhang, P.: A markerless human–robot interface using particle filter and Kalman filter for dual robots. IEEE Trans. Ind. Electron. **62**(4), 2257–2264 (2014)

Enan, S.S., Fulton, M., Sattar, J.: Robotic detection of a human-comprehensible gestural language for underwater multi-human–robot collaboration. arXiv preprint arXiv:2207.05331 (2022)

Granqvist, C.G., Avendaño, E., Azens, A.: Electrochromic coatings and devices: survey of some recent advances. Thin Solid Films **442**(1–2), 201–211 (2003)

Grasse, L., Boutros, S.J., Tata, M.S.: Speech interaction to control a hands-free delivery robot for high-risk health care scenarios. Front. Robot. AI **8**, 612750 (2021)

Gummadi, R., Wetherall, D., Greenstein, B., Seshan, S.: Understanding and mitigating the impact of rf interference on 802.11 networks. ACM SIGCOMM Comput. Commun. Rev. **37**(4), 385–396 (2007)

Hancock, P.A., Billings, D.R., Schaefer, K.E., Chen, J.Y., De Visser, E.J., Parasuraman, R.: A meta-analysis of factors affecting trust in human–robot interaction. Hum. Factors **53**(5), 517–527 (2011)

Hedayati, H., Walker, M., Szafir, D.: Improving collocated robot teleoperation with augmented reality. In: Proceedings of the 2018 ACM/IEEE International Conference on Human–Robot Interaction, pp. 78–86 (2018)

Hu, C., Ma, D., Hassan, M., Hu, W.: Nlc: natural light communication using switchable glass. In: IEEE INFOCOM 2020-IEEE Conference on Computer Communications Workshops (INFOCOM WKSHPS), pp. 201–206. IEEE (2020)

Hu, Z., Marshall, C., Bicker, R., Taylor, P.: Automatic surface roughing with 3d machine vision and cooperative robot control. Robot. Auton. Syst. **55**(7), 552–560 (2007)

Islam, M.J., Ho, M., Sattar, J.: Dynamic reconfiguration of mission parameters in underwater human–robot collaboration. In: 2018 IEEE International Conference on Robotics and Automation (ICRA), pp. 6212–6219. IEEE (2018)

Islam, M.J., Ho, M., Sattar, J.: Understanding human motion and gestures for underwater human–robot collaboration. J. Field Robot. **36**(5), 851–873 (2019)

Keyes, B., Micire, M., Drury, J.L., Yanco, H.A., Chugo, D.: Improving human–robot interaction through interface evolution. In: Human–Robot Interaction, pp. 183–202. InTech (2010)

Lai, K.-Y., Chen, W.-T., Wu, Y.-H., Chen, Y.-F., Tsai, J.-c.: 3D-printed and pdlc-tuned corner cube retroreflector for sunlight communication. In: 2019 International Conference on Optical MEMS and Nanophotonics (OMN), pp. 164–165. IEEE (2019)

Lampert, C.M.: Smart switchable glazing for solar energy and daylight control. Sol. Energy Mater. Sol. Cells **52**(3–4), 207–221 (1998)

Li, J., Liu, A., Shen, G., Li, L., Sun, C., Zhao, F.: Retro-VLC: enabling battery-free duplex visible light communication for mobile and iot applications. In: Proceedings of the 16th International Workshop on Mobile Computing Systems and Applications, pp. 21–26 (2015)

Magnago, V., Palopoli, L., Buffi, A., Tellini, B., Motroni, A., Nepa, P., Macii, D., Fontanelli, D.: Ranging-free uhf-rfid robot positioning through phase measurements of passive tags. IEEE Trans. Instrum. Meas. **69**(5), 2408–2418 (2019)

Mateo, C., Brunete, A., Gambao, E., Hernando, M.: Hammer: an android based application for end-user industrial robot programming. In: 2014 IEEE/ASME 10th International Conference on Mechatronic and Embedded Systems and Applications (MESA), pp. 1–6. IEEE (2014)

Nathan, A., Ahnood, A., Cole, M.T., Lee, S., Suzuki, Y., Hiralal, P., Bonaccorso, F., Hasan, T., Garcia-Gancedo, L., Dyadyusha, A.,

et al.: Flexible electronics: the next ubiquitous platform. In: Proceedings of the IEEE 100 (Special Centennial Issue), pp. 1486–1517 (2012)
Punnoose, R.J., Tseng, R.S., Stancil, D.D.: Experimental results for interference between Bluetooth and IEEE 802.11 b DSSS systems. In: IEEE 54th Vehicular Technology Conference. VTC Fall 2001. Proceedings (Cat. No. 01CH37211), vol. 1, pp. 67–71. IEEE (2001)
Qin, K., Chen, C., Pu, X., Tang, Q., He, W., Liu, Y., Zeng, Q., Liu, G., Guo, H., Hu, C.: Magnetic array assisted triboelectric nanogenerator sensor for real-time gesture interaction. Nano-micro Lett. **13**(1), 1–9 (2021)
Quintero, C.P., Li, S., Pan, M.K., Chan, W.P., Van der Loos, H.M., Croft, E.: Robot programming through augmented trajectories in augmented reality. In: 2018 IEEE/RSJ International Conference on Intelligent Robots and Systems (IROS), pp. 1838–1844. IEEE (2018)
Ramzan, A., Rehman, S., Perwaiz, A.: RFID technology: beyond cash-based methods in vending machine. In: 2017 2nd International Conference on Control and Robotics Engineering (ICCRE), pp. 189–193. IEEE (2017)
Shao, S., Khreishah, A., Elgala, H.: Pixelated VLC-backscattering for self-charging indoor IoT devices. IEEE Photonics Technol. Lett. **29**(2), 177–180 (2016)
Solvang, B., Sziebig, G., Korondi, P.: Robot programming in machining operations. In: Robot Manipulators, pp. 479–496. I-Tech, Vienna, Austria (2008)
Stadler, S., Kain, K., Giuliani, M., Mirnig, N., Stollnberger, G., Tscheligi, M.: Augmented reality for industrial robot programmers: workload analysis for task-based, augmented reality-supported robot control. In: 2016 25th IEEE International Symposium on Robot and Human Interactive Communication (RO-MAN), pp. 179–184. IEEE (2016)
Van den Bergh, M., Carton, D., De Nijs, R., Mitsou, N., Landsiedel, C., Kuehnlenz, K., Wollherr, D., Van Gool, L., Buss, M.: Real-time 3d hand gesture interaction with a robot for understanding directions from humans. In: 2011 Ro-Man, pp. 357–362. IEEE (2011)
Vergaz, R., Pena, J., Barrios, D., Pérez, I., Torres, J.: Electrooptical behaviour and control of a suspended particle device. Opto-Electron. Rev. **15**(3), 154–158 (2007)
Villani, V., Sabattini, L., Riggio, G., Secchi, C., Minelli, M., Fantuzzi, C.: A natural infrastructure-less human–robot interaction system. IEEE Robot. Autom. Lett. **2**(3), 1640–1647 (2017)
Walker, M., Hedayati, H., Lee, J., Szafir, D.: Communicating robot motion intent with augmented reality. In: Proceedings of the 2018 ACM/IEEE International Conference on Human–Robot Interaction, pp. 316–324 (2018)
Wang, P., Feng, L., Chen, G., Xu, C., Wu, Y., Xu, K., Shen, G., Du, K., Huang, G., Liu, X.: Renovating road signs for infrastructure-to-vehicle networking: a visible light backscatter communication and networking approach. In: Proceedings of the 26th Annual International Conference on Mobile Computing and Networking, pp. 1–13 (2020)
Wu, Y., Wang, P., Xu, K., Feng, L., Xu, C.: Turboboosting visible light backscatter communication. In: Proceedings of the Annual Conference of the ACM Special Interest Group on Data Communication on the Applications, Technologies, Architectures, and Protocols for Computer Communication, pp. 186–197 (2020)
Xu, X., Shen, Y., Yang, J., Xu, C., Shen, G., Chen, G., Ni, Y.: Passivevlc: enabling practical visible light backscatter communication for battery-free IOT applications. In: Proceedings of the 23rd Annual International Conference on Mobile Computing and Networking, pp. 180–192 (2017)
Yang, J.: Apparatus and method for suppressing interference caused by coexistence of WiMAX and WiFi. Google Patents. US Patent 8,553,622 (2013)
Yang, H.-D., Park, A.-Y., Lee, S.-W.: Gesture spotting and recognition for human–robot interaction. IEEE Trans. Rob. **23**(2), 256–270 (2007)
Zhang, H., Chen, H., Xi, N., Zhang, G., He, J.: On-line path generation for robotic deburring of cast aluminum wheels. In: 2006 IEEE/RSJ International Conference on Intelligent Robots and Systems, pp. 2400–2405. IEEE (2006)

Wei Li is currently a third-year master student in School of Computer Science at Peking University. Before joining the master program, he received his bachelor degree at Beijing University of Posts and Telecommunications. His research interests include RF sensing, acoustic sensing and optical human-computer interaction systems.

Tuochao Chen is currently a first-year PhD student in Paul G. Allen School of Computer Science & Engineering at University of Washington advised by Professor Shyam. His research interest includes ubiquitous computing, mobile systems and intelligent sensing technology.

Zhe Ou is a junior undergraduate student in School of Physics at Peking University, with a double major in Computer Science. His research interests focus on wireless communication systems and embedded systems.

Xin Wen is currently a second-year master student in School of Mathematics and Computer Science at NanChang University. His research interests include Distributed systems, Serverless optimization.

Zichen Xu is a Professor and associate dean of the School of Mathematics and Computer Science, Nanchang University, Nanchang, China. He is among The 1st selected Jiangxi Provincial Thousand Young Talents. His research interests are in the area of computing system design in the development of providing sustainable data services in unreliable/unstable systems. He received the B.S. degree from the Beijing University of Posts and Telecommunications, Beijing, China, in 2007, and the Ph.D. degree from The Ohio State University, Columbus, OH, USA, in 2016.

Chenren Xu is an Endowed Boya Young Fellow Associate Professor (with early tenure) and Deputy Director of Institute of Networking and Energy-efficient Computing in the School of Computer Science at Peking University (PKU). He directs PKU Software-hardware Orchestrated ARchitecture (SOAR) Lab and enjoys inventing future mobile technologies spanning across wireless, networking and system with his students to bring digital intelligence to transportation, logistics, manufacturing and health domains for better efficiency and user experience. He is the General Secretary of ACM SIGBED China, Executive Committee of ACM SIGBED and SIGMOBILE, Editor of ACM IMWUT. He published papers and has been serving as organization committee and/or TPC in venues including SIGCOMM, MobiCom, NSDI, SenSys and INFOCOM.